ACS OMEGA

http://pubs.acs.org/journal/acsodf

Article

# Investigation on the Direct and Bystander Effects in HeLa Cells Exposed to Very Low $\alpha$-Radiation Using Electrical Impedance Measurement

AbdulMojeed O. Ilyas,* Md Kowsar Alam, Jamal-Deen Musah, Mengsu Yang, Yun Wah Lam, Vellaisamy A. L. Roy, and Condon Lau

Cite This: *ACS Omega* 2021, 6, 13995−14003

Read Online

ACCESS | Metrics & More | Article Recommendations

**ABSTRACT:** The impact of radiation-induced bystander effect (RIBE) is still not well understood in radiotherapy. RIBEs are biological effects expressed by nonirradiated cells near or far from the irradiated cells. Most radiological studies on cancer cells have been based on biochemical characterization. However, biophysical investigation with label-free techniques to analyze and compare the direct irradiation effect and RIBE has lagged. In this work, we employed an electrical cell-indium tin oxide (ITO) substrate impedance system (ECIIS) as a bioimpedance sensor to evaluate the HeLa cells' response. The bioimpedance of untreated/nonirradiated HeLa (N-HeLa) cells, $\alpha$-particle (Am-241)-irradiated HeLa (I-HeLa) cells, and bystander HeLa (B-HeLa) cells exposed to media from I-HeLa cells was monitored with a sampling interval of 8 s over a period of 24 h. Also, we imaged the cells at times where impedance changes were observed. Different radiation doses (0.5 cGy, 1.2 cGy, and 1.7 cGy) were used to investigate I-HeLa and B-HeLa cells' radiation-dose-dependence. By analyzing the changes in absolute impedance and cell size/number with time, compared to N-HeLa cells, B-HeLa cells mimicked the I-HeLa cells' damage and modification of proliferation rate. Contrary to the irradiated cells, the bystander cells' damage rate and proliferation rate enhancements have an inverse radiation-dose-response. Also, we report multiple RIBEs in HeLa cells in a single measurement and provide crucial insights into the RIBE mechanism without any labeling procedure. Unambiguously, our results have shown that the time-dependent control of RIBE is important during $\alpha$-radiation-based radiotherapy of HeLa cells.

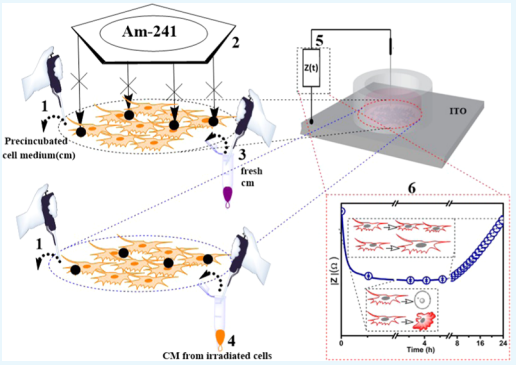


## INTRODUCTION

In modern medicine, cancer is a significant health problem that is second to heart disease in the cause of death worldwide.[1] Cases of cancer are projected to more than double worldwide in the next 20−40 years.[1,2] The International Agency for Research on Cancer (IARC) predicted that 17 million cancer deaths and 26 million new cancer cases would occur worldwide by 2030.[3] One of the integral and essential parts of cancer management, which confers most survival benefits, is radiotherapy or radiation therapy, which uses high-energy radiation to destroy cancer cells.[4] The treatment of localized malignant tumors in approximately 50% of patients requires radiation.[4] In recent years, identifying the radiation-induced bystander effect (RIBE) has challenged the general belief of how radiation directly or indirectly damages cells. In RIBE, the nonirradiated cells near or far from irradiated cells demonstrate similar responses to those of the irradiated cells.[4] RIBE's implication in radiation therapy is essential, and its impact is gradually growing in radiation oncology.[4] In the past two decades, RIBEs observed in nonirradiated cells include cell death, delay in the cell cycle, micronuclei formation, mutations, induction of sister chromatid exchanges, cell growth stimulation, and DNA damage.[4] Investigations done on the mechanism controlling RIBE have recognized possible signaling pathways. The RIBE signals released by irradiated cells were received by both distant and neighboring cells by diffusion of soluble factors in the medium or cellular gap-junction intercellular communication (GJIC).[5,6] Therefore, the nonirradiated cells are mixed with irradiated cells or treated with the medium collected from irradiated cells[7,8] in an in vitro study of RIBE. Several cell-based assays[9] and cell cytometry,[10] which require a cell staining buffer,[11,12] have been used as tools for RIBE analysis. A noninvasive and label-free technique useful for the real-time study of RIBE (as changes in the cell proliferation rate) is the

**Received:** December 3, 2020
**Accepted:** May 13, 2021
**Published:** May 26, 2021

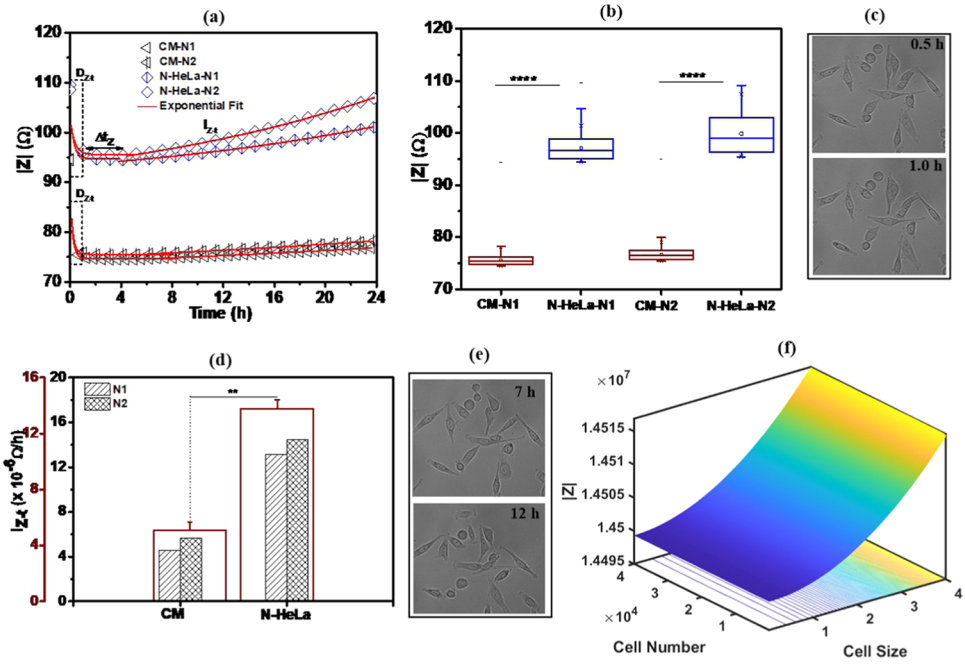


**Figure 1.** (a) Impedance-time spectra (|Z|-*t* spectra) of the cell medium and the N-HeLa cell. (b) The box plots comparing the average impedance data obtained for the cell medium and N-HeLa cells with the *p*-value obtained from comparing the pairs are indicated in the figure. (c) Cell event during the $D_{Z\text{-}t}$ of N-HeLa cells showing no change in cell size. (d) Comparison of the $slI_{Z\text{-}t}$ for CM and N-HeLa cells. (e) Microscopic image of the cell proliferation event in tagged cells for N-HeLa cells (cell division at 7 h and growth of divided cells at 12 h). $slI_{Z\text{-}t}$ is the slope obtained from exponential fitting of the increase in impedance with time. (f) Surface plot relating normalized total impedance |Z| with cell number and cell size at 4 kHz. Each bar represents the mean ± standard error of the mean (SEM) of two separate experiments ($n$ = 2). ** indicates $p < 0.01$ and **** indicates $p < 0.0001$.

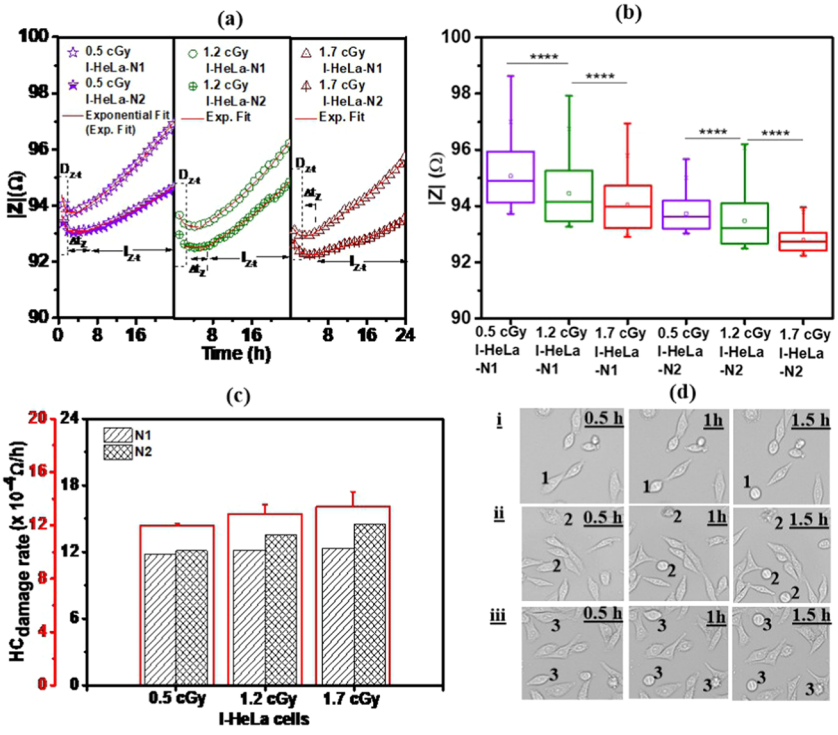


**Figure 2.** (a) Impedance-time spectra (|Z|-*t* spectra) of 0.5 cGy I-HeLa cells, 1.2 cGy I-HeLa cells, and 1.7 cGy I-HeLa cells. (b) The box plots compare the averages of impedance data over time for 0.5 cGy I-HeLa cells, 1.2 cGy I-HeLa cells, and 1.7 cGy I-HeLa cells with the obtained *p*-value for comparing the pairs indicated in the figure. (c) Comparison of the deduced $HC_{damage\ rate}$ for I-HeLa cells with varying radiation doses (0.5 cGy, 1.2 cGy, and 1.7 cGy). The $HC_{damage\ rate}$ represents the HeLa cell damage rate. (d) Microscopic image of the cell damage event (reduction in cell size) in number tagged cells for (i) 0.5 cGy I-HeLa cells, (ii) 1.2 cGy I-HeLa cells, and (iii) 1.7 cGy I-HeLa cells. Each bar represents the mean ± SEM of two separate experiments ($n$ = 2). **** indicates $p < 0.0001$.



https://doi.org/10.1021/acsomega.0c05888
*ACS Omega* 2021, 6, 13995−14003

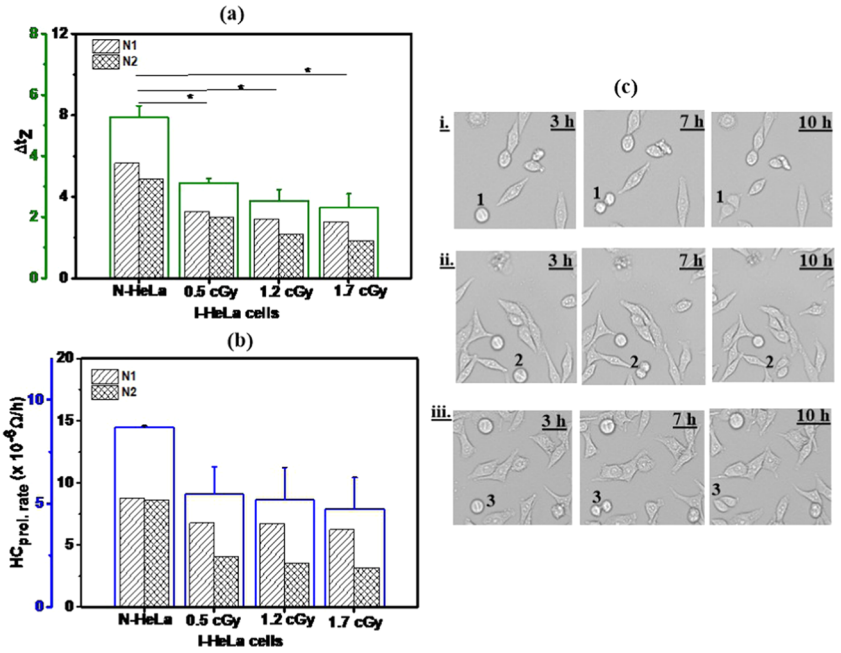


**Figure 3.** Comparison of the deduced (a) $\Delta t_Z$ and (b) $HC_{prol.\ rate}$ for I-HeLa cells with varying radiation doses (0.5 c Gy, 1.2 cGy, and 1.7 cGy). The $\Delta t_Z$ and $HC_{prol.\ rate}$ represent the changing time with constant impedance and the HeLa cell proliferation rate, respectively. (c) Microscopic image of the cell proliferation event in boxed cells for (i) 0.5 cGy I-HeLa cells, (ii) 1.2 cGy I-HeLa cells, and (iii) 1.7 cGy I-HeLa cells. Each bar represents the mean ± SEM of two separate experiments ($n$ = 2). * indicates $p < 0.05$.

impedance assay.[7] The procedure utilized in past impedance assay techniques[7,13−15] required long-duration sampling intervals (1 h), which limits the information acquired. Data collection, before the adhesion of cells to the sensing electrodes, hinders the observation of early RIBE. Lastly, an interdigitated gold plate electrode restricted the cell studies to a single cell,[7] making it challenging to maintain cell−cell communication. Thus, it is highly crucial to explain the impact of RIBE on far or near cancer cells during radiotherapy without using labeling procedures, which can affect cell behavior unexpectedly. To overcome these limitations, we used an electrical cell-indium tin oxide (ITO) substrate impedance system (ECIIS) with a temporal resolution of 8 s to continuously probe a large population of irradiated HeLa (I-HeLa) cells and bystander HeLa (B-HeLa) cells (nonirradiated HeLa (N-HeLa) cells treated with a cell medium (CM) acquired from I-HeLa cells) over a period of 24 h. This unique technique allows the quasi-real-time sensing of average biophysical changes in cells already adhered to an ITO substrate, thus enabling us to record the events immediately after exposure to radiation and bystander signals. For the first time, we report multiple RIBE (cell damage and enhanced cell proliferation rate) in a single measurement in a cancer cell model (HeLa cell).

## RESULTS

**Nonirradiated HeLa (N-HeLa) Cell and Cell Medium Measurement and System Simulation.** Figure 1a shows the impedance-time (|Z|-$t$) spectra of the cell medium (CM) and nonirradiated HeLa cells (N-HeLa) with a statistically significant difference ($p < 0.00001$) between the average impedance (|Z|) across time (Figure 1b). The first phase of the |Z|-$t$ spectra for both samples shows decreased impedance with time ($D_{Z\text{-}t}$). Since the microscopic image of N-HeLa cells (Figure 1c) during this time frame indicates no change in cell size, the $D_{Z\text{-}t}$ is only due to the system frequency scan to the preset frequency. After the $D_{Z\text{-}t}$, the N-HeLa cells show a constant impedance, which is represented with $\Delta t_Z$ before the impedance increases with time. The slope of the increasing impedance with time ($sI_{Z\text{-}t}$) for N-HeLa cells is significantly higher than that of CM (Figure 1d), and this indicates the contribution of cell proliferation because the microscopic image of the cell event at this phase shows an increase in N-HeLa cell number and size (Figure 1e). Moreover, the surface plot obtained from our impedance system calculation shows that the increase in cell size and cell number contributes nonlinearly to the rise in absolute impedance (Figure 1f). Hence, our impedance system quantifies the proliferation of HeLa cells in real time.

**Irradiated HeLa Cell Measurement.** Figure 2a shows the |Z|-$t$ spectra of 0.5 cGy, 1.2 cGy, and 1.7 cGy $\alpha$-particle-irradiated HeLa (I-HeLa) cells with an early stage of $D_{Z\text{-}t}$ and $\Delta t_Z$ and a later stage $I_{Z\text{-}t}$. A statistically significant difference ($p < 0.00001$) was observed between the average impedance (|Z|) data across time (Figure 2b) for the paired comparisons (between 0.5 cGy I-HeLa and 1.2 cGy I-HeLa, between 0.5 cGy I-HeLa and 1.7 cGy I-HeLa cells, and between 1.2 cGy I-HeLa and 1.7 cGy I-HeLa cells). The $HC_{damage\ rate}$ deduced from $sD_{Z\text{-}t}$ from all I-HeLa cells increases with increasing radiation dose (Figure 2c). Hence, cell damage increases with an increase in radiation dose after irradiation. The microscopic images of the cell condition at $D_{Z\text{-}t}$ indicate a time-dependent reduction in the size of labeled cells influences the calculated cell damage rate (Figure 2d-i−iii).

After the $D_{Z\text{-}t}$, the obtained $\Delta t_Z$ values for all I-HeLa cells (Figure 3a) are smaller than N-HeLa cells. Moreover, the $\Delta t_Z$ becomes more shortened as the radiation dose increases. The $HC_{prolrate}$ deduced from $I_{Z\text{-}t}$ of all I-HeLa cells decreases as the radiation dose increases (Figure 3b). Hence, the proliferation rate of HeLa cells is suppressed as the radiation dose of the


https://doi.org/10.1021/acsomega.0c05888
ACS Omega 2021, 6, 13995−14003

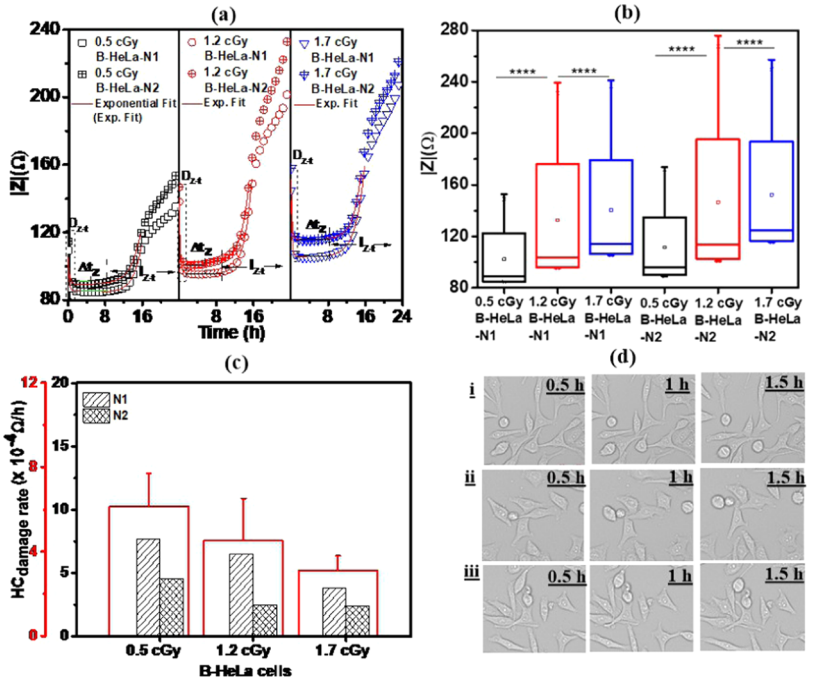


**Figure 4.** (a) Impedance-time spectra (|Z|-*t* spectra) of 0.5 cGy B-HeLa cells, 1.2 cGy B-HeLa cells, and 1.7 cGy B-HeLa cells. (b) The box plots compare the averages of impedance data over time for 0.5 cGy B-HeLa cells, 1.2 cGy B-HeLa cells, and 1.7 cGy B-HeLa cells with the obtained *p*-value for comparing the pairs indicated in the figure. (c) Comparison of the deduced $HC_{damage\ rate}$ for varying radiation doses. The $HC_{damage\ rate}$ represents the HeLa cell damage rate. (d) Microscopic image of the cell damage event (reduction in cell size) in number tagged cells for (i) 0.5 cGy B-HeLa cells, (ii) 1.2 cGy B-HeLa cells, and (iii) 1.7 cGy B-HeLa cells. Each bar represents the mean ± SEM of two separate experiments ($n = 2$). **** indicates $p < 0.0001$.

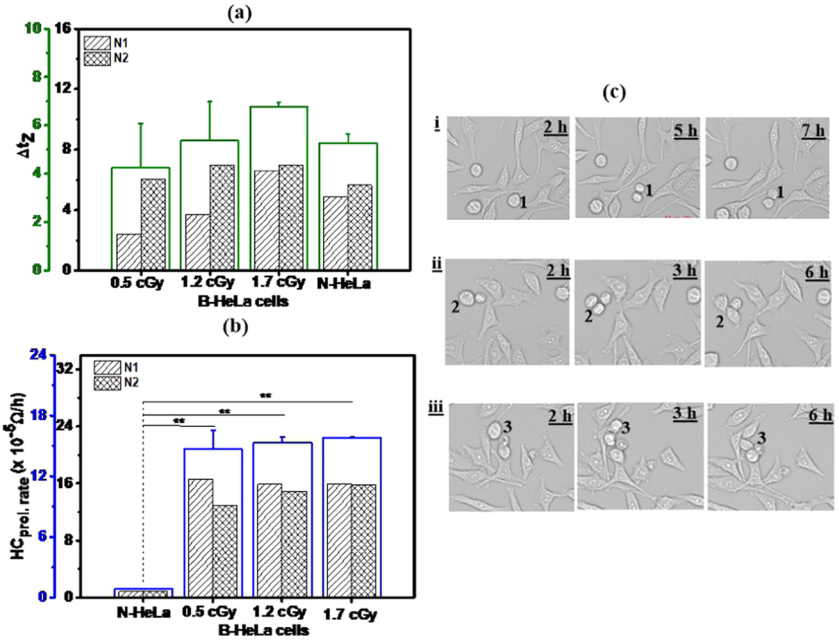


**Figure 5.** Comparison of the deduced (a) $\Delta t_Z$ and (b) $HC_{prol.\ rate}$ for B-HeLa cells with varying radiation doses (0.5 cGy, 1.2 cGy, and 1.7 cGy). The $\Delta t_Z$ and $HC_{prol.\ rate}$ represent the changing time with constant impedance and the HeLa cell proliferation rate, respectively. (c) Microscopic image of the cell proliferation event in tagged cells for (i) 0.5 cGy B-HeLa cells, (ii) 1.2 cGy B-HeLa cells, and (iii) 1.7 cGy B-HeLa cells. Each bar represents the mean ± SEM of two separate experiments ($n \geq 2$). ** indicates $p < 0.01$.

direct irradiation increases. The cells observed during $I_{Z\text{-}t}$ (Figure 3c-i–iii) show that cells double and increase in size with time.

**Bystander HeLa Cell Measurement.** The behaviors of 0.5 cGy bystander HeLa (B-HeLa), 1.2 cGy B-HeLa, and 1.7 cGy B-HeLa (N-HeLa cells treated with medium received from 0.5 cGy, 1.2 cGy, and 1.7 cGy I-HeLa cells) cells are translated into the |Z|-*t* spectra shown in Figure 4a. A statistically significant difference ($p < 0.00001$) was observed between the average impedance (|Z|) data across time (see


https://doi.org/10.1021/acsomega.0c05888
ACS Omega 2021, 6, 13995−14003

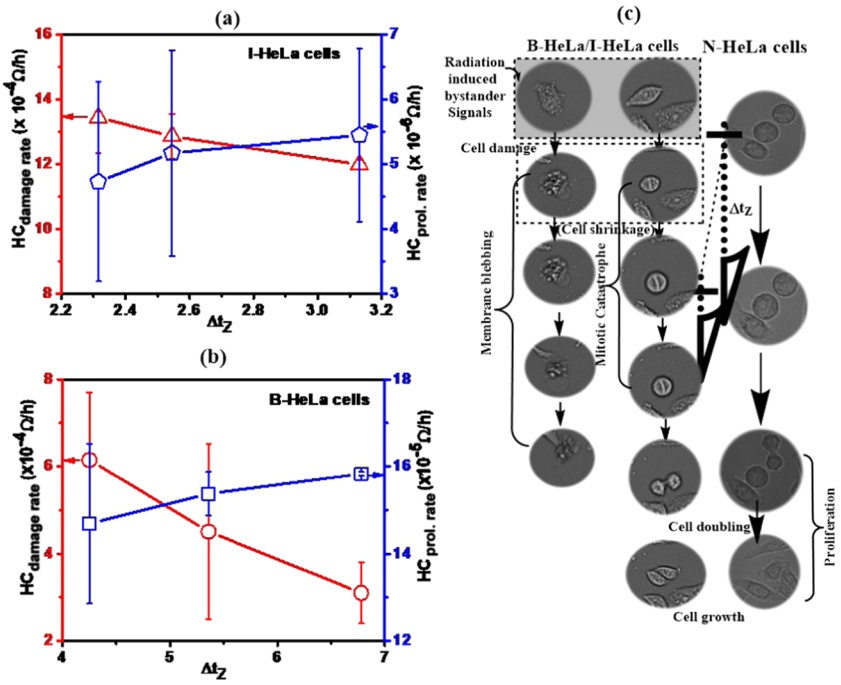


**Figure 6.** Interplay between the $\Delta t_Z$, $HC_{damage\ rate}$, and $HC_{prol.\ rate}$ for (a) I-HeLa cells and (b) B-HeLa cells. The $\Delta t_Z$, $HC_{damage\ rate}$, and $HC_{prol.\ rate}$ represent the changing time with constant impedance, the HeLa cell damage rate, and the HeLa cell proliferation rate, respectively. (c) I-HeLa and B-HeLa cells' mechanism. The HeLa cell damage is induced by treatment with the conditioned medium (ConM) or radiation. Some HeLa cells experience cell damage, while other cells evade this damaging process and enter a mode measured with $\Delta t_Z$ before commencing proliferation.

Figure 4b for the paired comparisons; between 0.5 cGy B-HeLa and 1.2 cGy B-HeLa cells, between 0.5 cGy B-HeLa and 1.7 cGy B-HeLa cells, and between 1.2 cGy B-HeLa and 1.7 cGy B-HeLa cells). The $HC_{damage\ rate}$ deduced from the $D_{Z\text{-}t}$ of all B-HeLa cells increases with a decrease in the radiation dose (Figure 4c). Hence, an inverse relationship occurs between cell damage and radiation dose, inducing the HeLa cell's bystander signals. The images of cells at $D_{Z\text{-}t}$ show that the number of tagged cells reduces in size with time and the population of labeled cells increases with a decrease in the radiation dose used on the donor cell (Figure 4d).

As a result, cell shrinkage influences the observed cell damage rate. The $\Delta t_Z$ values obtained after the $D_{Z\text{-}t}$ for all B-HeLa cells (Figure 5a) become more shortened as the radiation dose decreases from 1.7 cGy to 0.5 cGy. The $HC_{prolrate}$ deduced from the $I_{Z\text{-}t}$ of all B-HeLa cells increases with increasing radiation dose (Figure 5b). Hence, the proliferation of HeLa cells is increased by RIBE as the radiation dose increases. The cell events during $I_{Z\text{-}t}$ also show proliferation of the B-HeLa cells (Figure 5c), which include enlargement in cell size and the doubling of cells with time.

## DISCUSSION

Using a label-free technique, we have reported I-HeLa and B-HeLa cells' responses to ionizing radiation and RIBE, respectively, at 24 h real-time in vitro. It is evident from this study that (i) ECIIS can be used to monitor the real-time impact of irradiation and RIBE on cancer cells, (ii) the ECIIS method provides an easy way to observe the cell condition without the tedious labeling and counting process, (iii) the RIBE (cell damage and altered proliferation rate) is similar but disproportionate to the direct irradiation effect, and (iv) both RIBE and irradiation effect is time-dependent and radiation-dose-dependent.

With a radiation dose range of 0.5−1.7 cGy, most of the cells will be traversed by the $\alpha$ particles at the extranuclear components[16] and the average hit per nucleus will range between ∼0.035 and 0.117. This leads to a combined effect of direct irradiation[17,18] and indirect bystander effect in the I-HeLa cell population[19] mediated by only the presence of the cell medium.[20] Therefore, the RIBE observed and measured after conditioned medium (ConM) treatment will be a secondary radiation-induced bystander effect.[21,22]

The real-time shrinkage of cells deduced as $HC_{damage\ rate}$ observed in the $D_{Z\text{-}t}$ of I-HeLa and B-HeLa cells can only be associated with the exposure to ionizing radiation and RIBE because at this time frame, N-HeLa cells show no change. By obtaining microscopic images, we can deduce that the I-HeLa and B-HeLa cells undergo both early mitotic cell shrinkage (mitotic catastrophe)[23,24] and apoptotic cell shrinkage (shrinking cells with the blebbing membrane).[25,26] In our study, the B-HeLa cells experiencing cell damage indicate that radiation-induced bystander signals can kill cancer cells.[27,28] Clinically, radiotherapy also induces cancer cells' killing through the radiation-induced bystander signals.

We define the HeLa cell proliferation rate ($HC_{prol.rate}$) as the real-time increase in the HeLa cell size and HeLa cell doubling in our work. Compared to N-HeLa cells, $HC_{prol.rate}$ is reduced for I-HeLa cells but enhanced for B-HeLa cells. Hence, RIBE tends to counteract how irradiation's later-stage effect suppresses the cancer cell proliferation rate during cancer therapy. Thus, it is crucial to inhibit RIBE in a time-dependent manner to improve the efficacy of radiotherapy.

The constant impedance with changing time ($\Delta t_Z$) observed in N-HeLa cells shows that the cells are preparing for cell proliferation. Also, I-HeLa and B-HeLa cells pre-experiencing cell damage in the form of cell shrinkage evade the damaging process at $\Delta t_Z$ and prepare for cell proliferation.


https://doi.org/10.1021/acsomega.0c05888
ACS Omega 2021, 6, 13995−14003

From the relationship of the parameters ($HC_{damage\ rate}$, $\Delta t_Z$, and $HC_{prol.rate}$) in our results, which is similar for both I-HeLa cells (Figure 6a) and B-HeLa cells (Figure 6b), it can be explained that the $\Delta t_Z$ varies inversely with the $HC_{damage\ rate}$ but directly with the $HC_{prol.rate}$. Hence, we can deduce a mechanism for both B-HeLa and I-HeLa cells, as illustrated in Figure 6c. Briefly, the HeLa cell damage is induced by treatment with a conditioned medium (ConM) or radiation. Some HeLa cells evade this damaging process and enter a mode measured with $\Delta t_Z$, while other cells experience cell damage. Afterward, surviving cells began cell proliferation.

## CONCLUSIONS

We have shown that both direct irradiation and RIBE cause cell damage and alter the proliferation rate. Compared to past impedance-based RIBE experiments, we report two profound RIBEs (apoptotic cell death and enhanced cell proliferation) in our work due to the continuous real-time and short-time sampling interval approach of our experimental design. Also, we demonstrate that cell damage is not unique to irradiation but also influenced by RIBE at early time points. Also, at later time points, RIBE enhances cell proliferation rate at radiation dose ≥0.5 cGy. Our findings suggest that time-dependent control of cell proliferation is significant if RIBE's benefit is to be explored during radiotherapy. Hence, our work gives a better understanding of radiobiological processes during $\alpha$-radiation-based radiotherapy of HeLa cells.

## MATERIALS AND METHODS

**Cell Culture and Transfer from Stock to the Cell Compartment.** The HeLa cell line already prepared in a cell culture Petri dish was transferred to a cell compartment (cylindrical poly(dimethylsiloxane) (PDMS) well attached to the conductive side of ITO) for irradiation, medium treatment, and measurement in steps. Subsequently, the medium was removed from the cell culture Petri dish, and the cells were washed by 1× phosphate-buffered saline (PBS) to remove dead cells. Then, the cells were passaged by trypsinization to maintain a maximum confluence of 70%. Then, trypsin was removed, and Dulbecco's modified Eagle's medium (DMEM) supplemented with 10% fetal bovine serum (FBS) (Thermos Fisher Scientific, Hong Kong) was added to the cell suspension. Thus, $3.5 \times 10^5$ HeLa cells were seeded onto the indium tin oxide (ITO) substrate in the cell compartment. All steps were performed in the biosafety fume hood.

**Preparation of Nonirradiated Cells.** The $3.5 \times 10^5$ HeLa cells were seeded onto an ITO substrate at the bottom of a PDMS well (cell compartment) and then incubated for 17.5 ± 0.5 h. The preincubation cell medium in the PDMS wells was removed and replaced with a fresh medium before being placed in the incubator for impedance measurement.

**Preparation of Irradiated Cells.** The irradiation of the cells served two purposes in the present investigation. First, it was to prepare irradiated cells on which the effect of irradiation would be studied over 24 h in real time. The second was to prepare a conditioned medium (ConM), which had conditioned the B-HeLa cells. The HeLa cells were first seeded and incubated for 17.5 ± 0.5 h. The preincubation medium was removed from the cell compartment before the cells were exposed to Am-241 radiation. In the radiation procedure, we place the disk type $\alpha$-radiation source on top of the cell compartment at a distance dependent on the height of the cylindrical PDMS attached to the surface of the ITO substrate with adherent cells. The irradiation source used was Americium-241 (Am-241). Considering the air gap between the $\alpha$-radiation source and the cells, the absence of vacuum allowed energy loss to occur.[29] Hence, the average $\alpha$ particle energy was <5.18 MeV, activity was 0.0087 $\mu$Ci, and dose rate was 0.1742 cGy/min, as confirmed experimentally using an $\alpha$-radiation detector at 12 mm distance with an air gap to the $\alpha$-radiation source connected to a multichannel analyzer and a computer using maestro software. After irradiation, a fresh cell medium was added to the cells and taken to the measurement incubator. Moreover, the exposure time of the cells to the $\alpha$-radiation source was adjusted to vary the amount of absorbed dose by the adherent cells. The average hit per nucleus of the radiation dose ($D$) incident on the Hela cell nucleus was calculated after the fluence ($F$) was deduced from eq 1.

$$D[\mathrm{Gy}] = 0.16 \times F[\mathrm{particle/\mu m^2}] \times L\ [\mathrm{keV/\mu m}] \times (1/\rho) \quad (1)$$

where $L$ is the linear energy transfer (LET) of Am-241 incident to the cells (125 keV/$\mu$m) and $\rho$ is the density of the cell (assumed as 1 g/cm$^3$).[30]

**RIBE Experiment.** The RIBE experiment involved the transfer of the culture medium from irradiated HeLa (I-HeLa) cells to nonirradiated HeLa (N-HeLa) cells, known as bystander HeLa (B-HeLa) cells. The cell concentration ratio of the donor I-HeLa cells and N-HeLa cells treated with CM (B-HeLa) was kept at 5:1. The cells to be irradiated were first seeded in a Petri dish for 17.5 ± 0.5 h. The preincubated cell culture medium (P-cm) was removed from the cells to avoid direct effects of radiation on the medium. The I-HeLa cells were exposed to 0.5 cGy, 1.2 cGy, and 1.7 cGy radiation doses of Am-241 using the radiation source described in the previous section. After irradiation, the fresh cell medium was filled into the Petri dish and removed after 3 min from the 0.5 cGy, 1.2 cGy, and 1.7 cGy I-HeLa cells, filtered through a 0.22 $\mu$m filter, and kept as the conditioned medium (ConM). The N-HeLa cells seeded and incubated beforehand in a cell compartment for 17.5 ± 0.5 h were then treated with the ConM by replacing the P-cm with the prepared ConM and taken for ECIIS measurement. The N-HeLa cells treated with the ConM obtained from the 0.5 cGy, 1.2 cGy, and 1.7 cGy I-HeLa cells are hereon referred to as 0.5 cGy, 1.2 cGy, and 1.7 cGy B-HeLa cells, respectively.

**ECIIS Measurement.** The electrical cell-indium tin oxide (ITO) substrate impedance system (ECIIS) measurement of the HeLa cells was carried out using an electrochemical workstation (CHI 660E) with three terminals and a cell compartment. The counter and reference electrode terminals were connected to a platinum wire inserted into a cell medium on top of the working electrode at the PDMS's bottom. The indium tin oxide (ITO; Luminescence Technology Corporation, Taiwan) electrode with HeLa cells adhered to the conductive surface served as the working electrode. The treatment of the ITO electrode surface for reducing cell mobility has been described in our previous work.[31] The HeLa cells prepared for different experimental purposes in the cell compartment were transferred to the incubator (37°C, 5% $CO_2$ atmosphere) for measurement. During the impedance measurement, we applied an AC voltage (0.005 V) at 4 kHz frequency, and the output data were obtained for 24 h in terms of the magnitude of the complex impedance (|Z|). After each experimental data, we discarded the cell compartment.


https://doi.org/10.1021/acsomega.0c05888
ACS Omega 2021, 6, 13995−14003

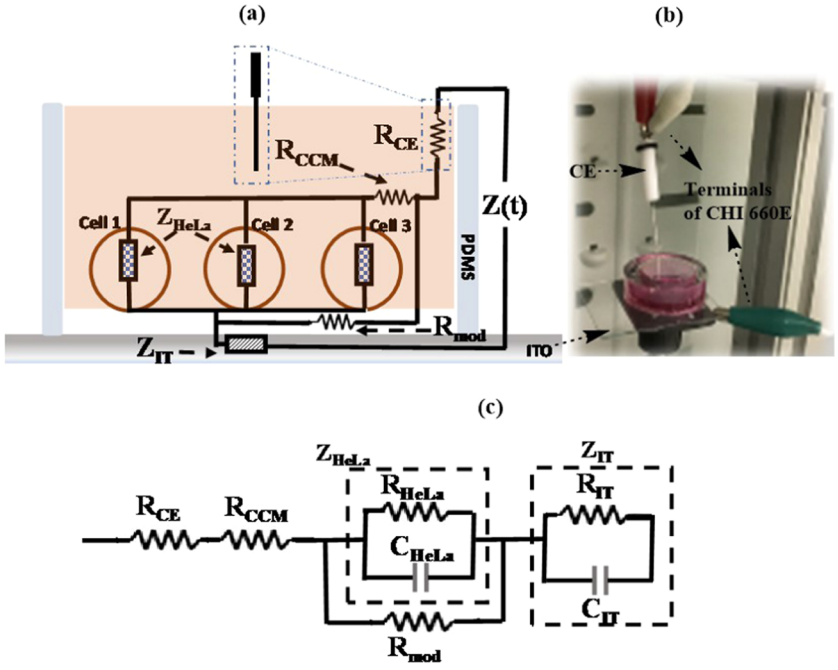


**Figure 7.** Configuration of our ECIIS system. (b) Image of the cell compartment connected to the terminals of the electrochemical workstation (CHI 660E). "Photograph courtesy of "AbdulMojeed O. Ilyas." Copyright 2021." (c) The equivalent circuit models $R_{CE}$, $R_{CCM}$, $R_{HeLa}$, $R_{mod}$, and $R_{IT}$ are the resistances of the platinum wire counter electrode (CE), the cell medium, the HeLa cell, the cell to the working electrode, and the indium tin oxide (ITO) working electrode, respectively. are the $C_{HeLa}$ and $C_{IT}$ are the capacitances of the HeLa cell membrane and the ITO electrode conductive surface, respectively.

**Cell Damage Rate and Cell Proliferation Rate Estimation.** The probing of adherent cells in our impedance system made it a requirement for the impedance to vary in the following ways. First, the impedance decreased ($D_{Z\text{-}t}$) as the system scanned toward the preset frequency of 4 kHz ($f_{SC}$)[32−34] and as the electrode coverage reduced with cell detachment or reduction in cell size.[35] Cell detachment and a decrease in cell size indicated the initiation of cell damage.[36] The cell damage rate ($HC_{damage\ rate}$) (the rate at which a cell shrinks or detaches) was deduced using eq 2.

$$HC_{damage\ rate} = sD_{Z-t}(\text{I} - \text{H and B} - \text{H}) - sD_{Z-t}(\text{N} - \text{H}) \quad (2)$$

Here, $sD_{Z\text{-}t}$ (I-H and B-H) and $sD_{Z\text{-}t}$ (N-H) are the slopes obtained from exponential fitting of the $D_{Z\text{-}t}$ of I-HeLa cells/B-HeLa cells and N-HeLa cells, respectively.

Second, the change in time with constant impedance ($\Delta t_Z$) occurred when there was no cell size change. The impedance increased ($I_{Z\text{-}t}$) due to adherent cell proliferation (cell growth and cell division) on the working electrode. Hence, the cell proliferation rate ($HC_{prol\ rate}$) was deduced using eq 3.

$$HC_{prol\ rate} = sI_{Z-t}(\text{HC}) - sI_{Z-t}(\text{CM}) \quad (3)$$

Here, $sI_{Z\text{-}t}$ (HC) and $sI_{Z\text{-}t}$ (CM) are the slopes obtained from exponential fitting of the increasing impedance of N-HeLa cells and CM. The $D_{Z\text{-}t}$ and $I_{Z\text{-}t}$ were quantified by deducing the slope from the nonlinear decreasing and increasing impedance with time. The slope was deduced from the nonlinear decrease and increase in impedance by the exponential function fitting with Origin 9.0 software, which used eq 4.

$$Z = Ae^{\pm\mu t} \quad (4)$$

$$\ln Z = \ln A \pm \mu t \quad (5)$$

The linearized exponential function (eq 5) shows the plot of $\ln Z$ versus $t$ (real experimental time), where $\pm\mu$ is the slope and $\ln A$ is the intercept. We considered the exponential fit valid if the $r^2$ was higher than 0.97. Hence, $+\mu$ is the slope from an increase in impedance with time ($slI_{Z\text{-}t}$) and $-\mu$ is the slope from a decrease in impedance with time ($slD_{Z\text{-}t}$).

**Modeling the ECIIS System.** In our ECIIS system, the counter electrode (platinum wire) was inserted and held at the top and the working electrode (ITO) was at the bottom with the electrolyte (cell culture medium (CCM)) in between the electrodes. Therefore, the impedance of the counter electrode was in series with the impedance of the cell culture medium, the cell population, and the ITO working electrode. The configuration representing the presence of cells with the cell medium is shown in Figure 7a using the image of the physical electrochemical setup shown in Figure 7b. The $Z_{total}$ in eq 6 was deduced from the obtained equivalent circuit (Figure 7c) using Kirchhoff's laws, and the components are defined in eqs 7−11.

$$Z_{total} = R_{CE} + R_{ccm} + Z_{cells} + Z_{IT} \quad (6)$$

$$Z_{cells} = \frac{\sum_{i=1}^{n} R_{mod} \times \sum_{i=1}^{n} Z_{HeLa}}{\sum_{i=1}^{n} R_{mod} + \sum_{i=1}^{n} Z_{HeLa}} \quad (7)$$

$$R_{CCM} = \frac{L_{ccm}}{\sigma\pi r_{ito}^{2}} \quad (8)$$

$$R_{CE} = \frac{L_{CE}\,\rho_{CE}}{\pi r_{PE}^{2}} \quad (9)$$

$$R_{mod} = \frac{\rho_{ccm}}{\theta\pi d} \quad (10)$$



https://doi.org/10.1021/acsomega.0c05888
ACS Omega 2021, 6, 13995−14003

$$C_{IT} = \frac{\varepsilon_0 \varepsilon_{r-ito} \pi r_{ito}^{\ 2}}{t_{ito}} \quad (11)$$

In the model, $Z_{ITO}$, $Z_{Cells}$, and $Z$ are the working electrode (ITO) impedance, HeLa cells, and total impedance, respectively. The $R_{CCM}$ (the resistance of the CCM), $R_{CE}$ (resistance of the counter electrode), $R_{mod}$ (the cell to ITO resistance), and $C_{IT}$ (the ITO capacitance) are defined with eqs 7−10, respectively. The cells were assumed to be spherical and were modeled as a resistor (cytoplasm) in series with a capacitor (cell membrane). In the simulation, the resistance of the ITO ($R_{IT}$), the electrical permittivity of free space ($\varepsilon_0$), the relative permittivity of the ITO substrate ($\varepsilon_{r\text{-}ito}$), the radius of the ITO substrate ($r_{ito}$), the radius of the platinum wire ($r_{CE}$), and the conductivity of the CCM ($\rho_{ccm}$) were 1767 Ω, $8.854 \times 10^{-14}$ C/(Vcm), 0.541, 0.2 cm, 0.5 μm, and 100 Ω·cm, respectively. The variation between the compared quantities was obtained using MATLAB R2019b. A core i5 with a 1.6 GHz processor with 8.00 GB memory obtained a solution in 2−5 min.

**Microscope Image Acquisition.** Bright-field images for illustrating cell events at $D_{Z\text{-}t}$ and $I_{Z\text{-}t}$ were acquired using a 20×/NA 0.75 dry objective with an Etaluma LS720 microscope.

**Statistical Analysis.** We used Origin Pro 9.0 to perform all statistical analyses and presented the impedance |Z| data collected across time from all of the experiments in terms of their means and standard deviations. We assessed the differences between the means of the data using one-way analysis of variance (ANOVA) (for comparing > 2 samples) and Student's *t*-test (for comparing two samples). Turkey's test was also used in conjunction with ANOVA (post hoc analysis) to find the significant difference between the groups' means. A *p*-value of ≤0.05 was taken as a significant difference between the compared groups.

## AUTHOR INFORMATION


### Corresponding Author

**AbdulMojeed O. Ilyas** − *Department of Physics, City University of Hong Kong, Kowloon 999077, Hong Kong SAR, China; Department of Physics, Federal University Oye-Ekiti, Oye-Ekiti, Ekiti State 3600001, Nigeria;* orcid.org/0000-0001-8304-6888; Email: amoilyas2-c@my.cityu.edu.hk

### Authors

**Md Kowsar Alam** − *Department of Biomedical Sciences, City University of Hong Kong, Kowloon 999077, Hong Kong SAR, China; Department of Physics, University of Chittagong, Chittagong 4331, Bangladesh*

**Jamal-Deen Musah** − *Department of Material Science and Engineering and State Key Laboratory of Terahertz and Millimeter Waves, City University of Hong Kong, Kowloon 999077, Hong Kong SAR, China*

**Mengsu Yang** − *Department of Biomedical Sciences, City University of Hong Kong, Kowloon 999077, Hong Kong SAR, China*

**Yun Wah Lam** − *Department of Chemistry, City University of Hong Kong, Kowloon 999077, Hong Kong SAR, China*

**Vellaisamy A. L. Roy** − *James Watt School of Engineering, University of Glasgow, Glasgow G12 8QQ, United Kingdom;* orcid.org/0000-0003-1432-9950

**Condon Lau** − *Department of Physics, City University of Hong Kong, Kowloon 999077, Hong Kong SAR, China*

Complete contact information is available at: https://pubs.acs.org/10.1021/acsomega.0c05888


### Notes

The authors declare no competing financial interest.

## ACKNOWLEDGMENTS

This work was supported by internal funding (from City University of Hong Kong).

## REFERENCES


(1) Siegel, R. L.; Miller, K. D.; Jemal, A.; Fuchs, H. E. Cancer Statistics, 2019. *Ca-Cancer J. Clin.* **2021**, *71*, 7−33.

(2) Thun, M. J.; DeLancey, J. O.; Center, M. M.; Jemal, A.; Ward, E. M. The Global Burden of Cancer: Priorities for Prevention. *Carcinogenesis* **2010**, *31*, 100−110.

(3) Solomon, S.; Mulugeta, W. Diagnosis and Risk Factors of Advanced Cancers in Ethiopia. *J. Cancer Prev.* **2019**, *24*, 163−172.

(4) Baskar, R.; Dai, J.; Wenlong, N.; Yeo, R.; Yeoh, K. W. Biological Response of Cancer Cells to Radiation Treatment. *Front. Mol. Biosci.* **2014**, *1*, No. 24.

(5) Zefferino, R.; Piccoli, C.; Di Gioia, S.; Capitanio, N.; Conese, M. Gap Junction Intercellular Communication in the Carcinogenesis Hallmarks: Is This a Phenomenon or Epiphenomenon? *Cells* **2019**, *8*, No. 896.

(6) Arora, S.; Heyza, J. R.; Chalfin, E. C.; Ruch, R. J.; Patrick, S. M. Gap Junction Intercellular Communication Positively Regulates Cisplatin Toxicity by Inducing Dna Damage through Bystander Signaling. *Cancers* **2018**, *10*, No. 368.

(7) Ibahim, M. J.; Crosbie, J. C.; Paiva, P.; Yang, Y.; Zaitseva, M.; Rogers, P. A. W. An Evaluation of Novel Real-Time Technology as a Tool for Measurement of Radiobiological and Radiation-Induced Bystander Effects. *Radiat. Environ. Biophys.* **2016**, *55*, 185−194.

(8) Burdak-Rothkamm, S.; Smith, A.; Lobachevsky, P.; Martin, R.; Prise, K. M. Radioprotection of Targeted and Bystander Cells by Methylproamine. *Strahlenther. Onkol.* **2015**, *191*, 248−255.

(9) Wang, H.; Yu, K. N.; Hou, J.; Liu, Q.; Han, W. Radiation-Induced Bystander Effect: Early Process and Rapid Assessment. *Cancer Lett.* **2015**, *356*, 137−144.

(10) Camplejohn, R. S. *Flow Cytometric Measurement of Cell Proliferation*; Brooks, S. A.; Schumacher, U., Eds.; Methods in Molecular Medicine; Humana Press, 2003; Vol. *57*, pp 133−143.

(11) Zhu, Z.; Frey, O.; Haandbaek, N.; Franke, F.; Rudolf, F.; Hierlemann, A. Time-Lapse Electrical Impedance Spectroscopy for Monitoring the Cell Cycle of Single Immobilized S. Pombe Cells. *Sci. Rep.* **2015**, *5*, No. 17180.

(12) Kakley, M.; Velle, K.; Fritz-Laylin, L. Relative Quantitation of Polymerized Actin in Suspension Cells by Flow Cytometry. *Bio-Protoc.* **2018**, *8*, No. e3094.

(13) Lepleux, C.; Marie-Brasset, A.; Temelie, M.; Boulanger, M.; Brotin, É.; Goldring, M. B.; Hirtz, C.; Varès, G.; Nakajima, T.; Saintigny, Y.; Savu, D.; Chevalier, F. Bystander Effectors of Chondrosarcoma Cells Irradiated at Different LET Impair Proliferation of Chondrocytes. *J. Cell Commun. Signaling* **2019**, *13*, 343−356.

(14) Atienza, J. M.; Yu, N.; Kirstein, S. L.; Xi, B.; Wang, X.; Xu, X.; Abassi, Y. A. Dynamic and Label-Freee Cell-Based Assays Using the Real-Time Cell Electronic Sensing System. *Assay Drug Dev. Technol.* **2006**, *4*, 597−607.

(15) Limame, R.; Wouters, A.; Pauwels, B.; Fransen, E.; Peeters, M.; Lardon, F.; de Wever, O.; Pauwels, P. Comparative Analysis of Dynamic Cell Viability, Migration and Invasion Assessments by Novel Real-Time Technology and Classic Endpoint Assays. *PLoS One* **2012**, *7*, No. e46536.

(16) Nagasawa, H.; Little, J. B. Induction of Sister Chromatid Exchanges by Extremely Low Doses of A-Particles. *Cancer Res.* **1992**, *52*, 6394−6396.
(17) Zhou, H.; Suzuki, M.; Randers-Pehrson, G.; Vannais, D.; Chen, G.; Trosko, J. E.; Waldren, C. A.; Hei, T. K. Radiation Risk to Low Fluences of Particles May Be Greater than We Thought. *Proc. Natl. Acad. Sci. U.S.A.* **2001**, *98*, 14410−14415.
(18) Wu, L. J.; Randers-Pehrson, G.; Xu, A.; Waldren, C. A.; Geard, C. R.; Yu, Z.; Hei, T. K. Targeted Cytoplasmic Irradiation with Alpha Particles Induces Mutations in Mammalian Cells. *Proc. Natl. Acad. Sci. U.S.A.* **1999**, *96*, 4959−4964.
(19) Kanagaraj, K.; Rajan, V.; Pandey, B. N.; Thayalan, K.; Venkatachalam, P. Primary and Secondary Bystander Effect and Genomic Instability in Cells Exposed to High and Low Linear Energy Transfer Radiations. *Int. J. Radiat. Biol.* **2019**, *95*, 1648−1658.
(20) Zhao, Y.; De Toledo, S. M.; Hu, G.; Hei, T. K.; Azzam, E. I. Connexins and Cyclooxygenase-2 Crosstalk in the Expression of Radiation-Induced Bystander Effects. *Br. J. Cancer* **2014**, *111*, 125−131.
(21) Dong, C.; He, M.; Tu, W.; Konishi, T.; Liu, W.; Xie, Y.; Dang, B.; Li, W.; Uchihori, Y.; Hei, T. K.; Shao, C. The Differential Role of Human Macrophage in Triggering Secondary Bystander Effects after Either Gamma-Ray or Carbon Beam Irradiation. *Cancer Lett.* **2015**, *363*, 92−100.
(22) Autsavapromporn, N.; Liu, C.; Kobayashi, A.; Ahmad, T. A. F. T.; Oikawa, M.; Dukaew, N.; Wang, J.; Wongnoppavichb, A.; Konishic, T. Emerging Role of Secondary Bystander Effects Induced by Fractionated Proton Microbeam Radiation. *Radiat. Res.* **2019**, *191*, 211−216.
(23) Vakifahmetoglu, H.; Olsson, M.; Zhivotovsky, B. Death through a Tragedy: Mitotic Catastrophe. *Cell Death Differ.* **2008**, *15*, 1153−1162.
(24) Castedo, M.; Perfettini, J. L.; Roumier, T.; Andreau, K.; Medema, R.; Kroemer, G. Cell Death by Mitotic Catastrophe: A Molecular Definition. *Oncogene* **2004**, *23*, 2825−2837.
(25) Dai, J.; Sheetz, M. P. Membrane Tether Formation from Blebbing Cells. *Biophys. J.* **1999**, *77*, 3363−3370.
(26) Woolley, T. E.; Gaffney, E. A.; Goriely, A. Membrane Shrinkage and Cortex Remodelling Are Predicted to Work in Harmony to Retract Blebs. *R. Soc. Open Sci.* **2015**, *2*, No. 150184.
(27) Heeran, A. B.; Berrigan, H. P.; O'Sullivan, J. N. The Radiation-Induced Bystander Effect (RIBE) and Its Connections with the Hallmarks of Cancer. *Radiat. Res.* **2019**, *192*, 668−679.
(28) Baskar, R. Emerging Role of Radiation Induced Bystander Effects: Cell Communications and Carcinogenesis. *Genome Integr.* **2010**, *1*, No. 13.
(29) Choppin, G. R.; Liljenzin, J.-O.; Rydberg, J. Detection and Measurement Techniques. In *Radiochemistry and Nuclear Chemistry*, 4th ed.; Gregory, C., Ed.; Academic Press: New York, 2002; pp 239−295.
(30) Esposito, G.; Antonelli, F.; Belli, M.; Campa, A.; Simone, G.; Sorrentino, E.; Tabocchini, M. A. An Alpha-Particle Irradiator for Radiobiological Research and Its Implementation for Bystander Effect Studies. *Radiat. Res.* **2009**, *172*, 632−642.
(31) Oo, S. L.; Venkatesh, S.; Ilyas, A. M.; Karthikeyan, V.; Arava, C. M.; Kong, E. Y.; Yeung, C. C.; Chen, X.; Yu, P. K. N.; Roy, V. A. L. Gating a Single Cell: A Label-Free and Real-Time Measurement Method for Cellular Progression. *Anal. Chem.* **2020**, *92*, 1738−1745.
(32) Gamal, W.; Wu, H.; Underwood, I.; Jia, J.; Smith, S.; Bagnaninchi, P. O. Impedance-Based Cellular Assays for Regenerative Medicine. *Philos. Trans. R. Soc., B* **2018**, *373*, No. 20170226.
(33) Hong, J. L.; Lan, K. C.; Jang, L. S. Electrical Characteristics Analysis of Various Cancer Cells Using a Microfluidic Device Based on Single-Cell Impedance Measurement. *Sens. Actuators, B* **2012**, *173*, 927−934.
(34) Martinez, J.; Montalibet, A.; McAdams, E.; Faivre, M.; Ferrigno, R. In *Effect of Electrode Material on the Sensitivity of Interdigitated Electrodes Used for Electrical Cell-Substrate Impedance Sensing Technology*, Proceedings of the Annual International Conference of the IEEE Engineering in Medicine and Biology Society, EMBS; IEEE, 2017; pp 813−816.
(35) Nahid, M. A.; Campbell, C. E.; Fong, K. S. K.; Barnhill, J. C.; Washington, M. A. An Evaluation of the Impact of Clinical Bacterial Isolates on Epithelial Cell Monolayer Integrity by the Electric Cell-Substrate Impedance Sensing (ECIS) Method. *J. Microbiol. Methods* **2020**, *169*, No. 105833.
(36) Caccamo, A. E.; Scaltriti, M.; Caporali, A.; D'Arca, D.; Scorcioni, F.; Astancolle, S.; Mangiola, M.; Bettuzzi, S. Cell Detachment and Apoptosis Induction of Immortalized Human Prostate Epithelial Cells Are Associated with Early Accumulation of a 45 KDa Nuclear Isoform of Clusterin. *Biochem. J.* **2004**, *382*, 157−168.


https://doi.org/10.1021/acsomega.0c05888
*ACS Omega* 2021, 6, 13995−14003